PAPER

Whiskey-phase exfoliation: exfoliation and printing of nanosheets using Irish whiskey

2D Materials

PAPER

RECEIVED
24 April 2019

REVISED
27 June 2019

ACCEPTED FOR PUBLICATION
5 August 2019

PUBLISHED
3 September 2019

Whiskey-phase exfoliation: exfoliation and printing of nanosheets using Irish whiskey

Adam G Kelly, Victor Vega-Mayoral, John B Boland and Jonathan N Coleman[1]

School of Physics, CRANN and AMBER Research Centres, Trinity College Dublin, Dublin 2, Ireland

[1] Author to whom any correspondence should be addressed.

E-mail: colemaj@tcd.ie

Keywords: liquid-phase exfoliation, 2D materials, printed electronics, whiskeytronics, graphene, tungsten disulfide, boron nitride

Supplementary material for this article is available online

Abstract

Recent advances in the liquid-phase exfoliation (LPE) of layered materials have facilitated significant progress in the creation of functional inks. While ethanol/water blends have been shown to yield reasonable nanosheet dispersions with the potential for refinement into printable inks, the exfoliated mass is typically too low for practical use. Here, we show that Irish whiskey can be used as a dispersant for nanosheets of graphene, BN and WS_2, yielding stable dispersions at reasonably high concentrations. We see some benefits compared to exfoliation in simple ethanol/water mixtures which we attribute to the presence of organic compounds in the whiskey. Size selection yields nanosheets which are relatively thin, with photoluminescence spectroscopy confirming the presence of monolayer tungsten disulfide (WS_2). We also show that whiskey-dispersed nanosheets of graphene and WS_2 can be printed into networks. These can be combined in heterostructures to produce thin-film transistors whose current can be modulated using ionic liquid (IL) gating. These devices show on:off ratios up to 340 and mobilities up to 1.5×10^{-3} $cm^2 V^{-1} s^{-1}$. The fact that these networks can be gated at all demonstrates the robustness of nanosheet networks against external additives while the mobility reported here should represent a performance-floor for future devices.

Introduction

Liquid-phase exfoliation (LPE) has become a widely-used technique for producing defect-free nanosheets from layered crystals [1–3]. LPE is very versatile, having been applied to a range of layered materials including graphene [3], MoS_2 [4], phosphorene [5] and even talc [6]. In addition, size-selection and monolayer enrichment protocols have yielded significant control over nanosheet dimensions [4, 7]. Once exfoliated, the nanosheets are typically stabilised via interactions with either the solvent itself or an additive, usually a surfactant or polymer [2, 8–10]. This confers a high degree of tunability and the refinement of such dispersions into functional inks is now growing rapidly [11–13]. However, as LPE is being used more and more in functional ink fabrication [5, 12, 14, 15], consideration must be given to the effect of additives on physical properties such as the mobility of printed nanosheet networks.

In the simplest case of solvent stabilisation, nanosheets are exfoliated, and subsequently stabilised, in solvents whose surface energy matches that of the nanosheets resulting in a low energetic cost of exfoliation [2, 3, 16]. However, it has also been shown that non-solvents (i.e. those with an unfavourable surface energy) can be mixed with other suitably mismatched solvents to give a mixture with the correct surface energy for exfoliation/stabilisation [17, 18]. Such solvent mixing can facilitate the tuning of rheology for printability [1] and can help avoid film redispersion when printing successive layers, in both cases without necessitating the addition of a binder [12]. Specifically, blends of water and ethanol have been shown to produce stable dispersions of graphene, WS_2 and MoS_2 with optimised stabilisation at 35–45 vol% of ethanol, although the mass produced is typically too low for integration into practical applications [17, 18].

From a particular perspective, the 35–45 vol% of ethanol is an interesting optimum as many commercial solvent blends, such as whiskey, contain solvent mixtures in this ratio. While the primary components of whiskey are ethanol and water, typically in a 40:60 ratio, whiskey also includes a broad combination of

esters, aldehydes, fusel alcohols and acids [19, 20], which are introduced during the extraction, fermentation and maturation processes (see SI S1 for more detail). The bulk of these compounds leach into the whiskey during cask maturation and, once bottled, are typically present in quantities of parts-per-million to parts-per-billion [21, 22]. It is possible that these natural additives will facilitate nanosheet stabilisation via steric stabilisation mechanisms [23] meaning whiskey should have an inherent advantage over other spirits such as vodka, which is nominally free of natural additives. We note that the use of unconventional liquid dispersion media is not uncommon as both coffee [24] and tea [25] have demonstrated reasonable exfoliation, although the produced nanosheets tend to be somewhat oxidised and produced at low yield.

While nanosheets stabilised using simply an ethanol/water blend or water with specific organic additives would naturally be more beneficial for creating a well controlled ink, we propose several reason why the complexity of the whiskey compound profile serves as a useful testbed for demonstrating the versatility of LPE and layered crystal networks. First, the organic compounds should complement the stability conferred by the ethanol/water blend, allowing the production of dispersions at printable nanosheet concentrations. Specifically, the presence of medium-to-long chain esters and lignin products should stabilise the nanosheets in a manner akin to polymer (steric) stabilisation [23] as the dispersion efficiency scales with the length of the molecular chain [26]. Second, it would be interesting to investigate the electrical properties of nanosheet networks in the presence of small amounts of additives to determine if their positive effect on stabilisation is outweighed by their (possible) negative effect on charge transport. Finally, and perhaps surprisingly, whiskey is both cheaper and less toxic (when administered responsibly) compared to prototypical exfoliating solvents such as NMP (€50 per litre for Teeling Small Batch Irish Whiskey versus €140 per litre for NMP Anhydrous from Sigma Aldrich).

In this study, we show that defect-free nanosheets can be exfoliated in Irish whiskey and also that inks produced in this manner can be printed into nanosheet networks for use in electronics. We exfoliated bulk powders of graphite, tungsten sulphide and boron nitride in Teeling whiskey (Teeling Small Batch, 46% alc/vol) and also in a 46:54 blend of ethanol/water as a control. The subsequent dispersions were then size-selected using liquid cascade centrifugation and the samples were analysed using spectroscopic and microscopic techniques to assess the quality of the whiskey-phase exfoliated (WPE) nanosheets. The inks of graphene and WS_2 were then printed using an aerosol jet printer to create high resolution side-gated transistors which allowed the quality of the networks to be assessed through the output and transfer curves. Here, we observe that the current in a network filled with a complex mix of additives can still be modulated with on:off ratios up to 340 with mobilities up to 1.5×10^{-3} $cm^2 V^{-1} s^{-1}$.

Results and discussion

Whiskey-phase exfoliation

Bulk powders of graphite, tungsten sulphide and boron nitride were exfoliated in whiskey or ethanol/water (46:54 vol:vol) using a standard procedure involving probe sonication and then size-selected by successive centrifugation as described in Methods and Materials. The WS_2 and boron nitride could be directly exfoliated and stabilised either using either Teeling whiskey or a 46:54 vol:vol blend of ethanol/water. However, graphite showed an extremely poor dispersion efficiency in both liquids. To address this, the graphite was first exfoliated in 1-methyl-2-pyrrolidone (NMP) and then solvent-exchanged to whiskey or ethanol/water following centrifugation (see Methods). Figure 1(A) shows each of the exfoliated materials dispersed in whiskey with a picture of the neat whiskey for comparison. Of these dispersions, we see that the colour of the boron nitride dispersion contains a visible influence from the whiskey compounds. Figure 1(B) shows representative TEM images of nanosheets collected from the whiskey-stabilised dispersions confirming successful exfoliation in all cases.

We assess the hypothesis that exfoliation efficiency might be enhanced using whiskey as a stabiliser by comparing whiskey-exfoliated dispersions with control samples exfoliated using a 46:54 blend of ethanol and water under identical conditions (see methods and materials). Figure 1(C) shows the obtained concentrations measured immediately after exfoliation, normalised to the concentration of the WPE sample. First, we note that the graphene sample in ethanol/water showed very low concentrations even when initially exfoliated in NMP and solvent-exchanged into the ethanol/water mixture. This is notable as nanosheets solvent-exchanged from NMP are usually stable at reasonable concentrations, likely due to adsorbed polymerised NMP [14, 27–29]. The inadequacy of both ethanol/water and whiskey as exfoliating solvents for graphite could be due to the evaporation of ethanol during the sonication process as this may significantly alter the 46:54 ethanol/water ratio (a thermally induced Angel's Share). The reports on graphene stabilised in an ethanol/water blend also show that the stability is sensitive to changes in this ratio [17] meaning an imbalance here could prevent efficient exfoliation. In contrast, after solvent exchange from NMP, the whiskey-phase graphene sample yields an appreciable concentration (0.47 mg ml^{-1}), roughly 100 times higher than that in ethanol/water sample. This provides some evidence that the whiskey compounds are stabilising the dispersion as the suboptimal 46:54 ethanol/water ratio can be overcome in whiskey but not ethanol/water alone. The WS_2 and BN are much less sensitive to such changes in the ethanol/water ratio

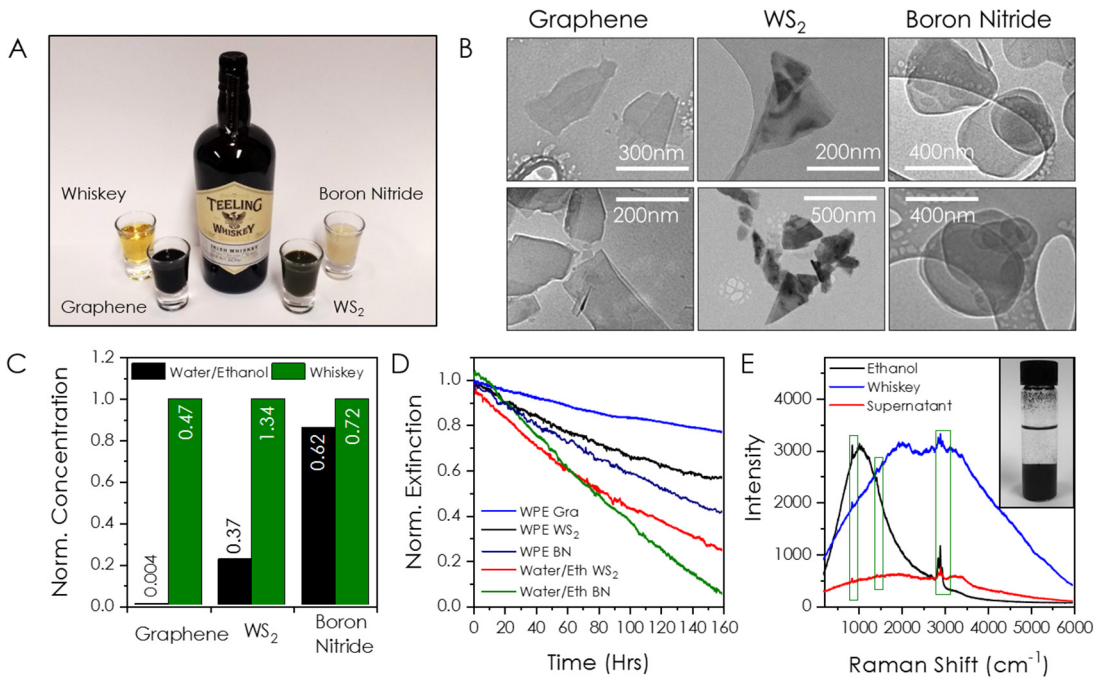

Figure 1. Material and exfoliation. (A) Image showing the whiskey-based inks contained in scientific glassware. (B) TEM imagery of the constituent nanosheets of each of the whiskey-based inks. (C) A bar chart showing the greater stability achieved using whiskey as a solvent over a 46:54 vol:vol ethanol/water blend. The abscissa is normalised to the concentration of the WPE ink, with the absolute concentrations shown in the bars (units: mg ml^{-1}). (D) The extinction over time of each material stabilised in whiskey and ethanol/water. The longest stability is seen for the whiskey-based inks. (E) The Raman spectra of ethanol, whiskey and the whiskey residual after exfoliating graphite. The absence of colour indicates that the whiskey compounds are adsorbed onto the nanosheets.

during sonication and yield reasonably high concentrations after direct exfoliation in ethanol/water. Nevertheless, the whiskey-exfoliated dispersions show higher concentrations in both cases. We note that the stability conferred by the whiskey compounds should be reproducible across increasingly aged batches as the vast majority of the compounds are added during the first three years of maturation [22].

We assessed the temporal stability of the samples using sedimentation measurements to monitor the optical extinction over time after exfoliation as shown in figure 1(D). Data for the graphene transferred to ethanol/water is not shown due to the complete flocculation of the dispersion within two hours. It is clear from the data in figure 1(D) that the most stable samples are those dispersed in whiskey. We propose that the increased concentration and stability observed in the whiskey-stabilised samples is due to the adsorption of organic molecules onto the surface of the nanosheets leading to steric stabilisation [23]. Evidence for such adsorption can be illustrated via the initial attempt to exfoliate graphite directly in whiskey. After sonication, the graphene rapidly reaggregates and sediments leaving the failed dispersion shown inset in figure 1(E). Critically, the supernatant is transparent, rather than the usual brown colour associated with whiskey (figure 1(A)). This indicates that the organic compounds have adsorbed on the graphene surfaces and been drawn into the sediment. To confirm this, we compared the Raman spectrum of the supernatant with that of ethanol and neat whiskey as shown in figure 1(E). The ethanol spectrum has a broad feature at ~1000 cm^{-1} and a set of sharp features at ~3000 cm^{-1}. In contrast, the Raman spectrum of pure whiskey is extremely broad, containing many contributions in addition to those associated with ethanol (highlighted in green). While the spectrum associated with the whiskey supernatant contains the ethanol/water feature, it is otherwise significantly reduced, especially at high wavenumber. This suggests that the organic compounds are no longer present in the supernatant and have been removed from dispersion along with the nanosheets.

Size-selection and optical characterisation of WPE nanosheets

A more complete characterisation of the WPE nanosheets can be achieved via spectroscopic analysis of size-selected fractions produced via liquid cascade centrifugation [7]. Here we focus on WPE-WS_2 due to the availability of metrics to estimate nanosheet size from optical spectra [7]. However, we also show some data from WPE-BN to show that such capabilities are not limited to WS_2. Comparison of the extinction spectra between the whiskey-exfoliated samples and the ethanol/water-exfoliated samples shows the whiskey-stabilised dispersions to display strong absorption at wavelengths <310 nm due to the presence of the organic compounds (see SI figure S2 (stacks.iop.org/TDM/6/045036/mmedia)). This is problematic as it limits our ability to perform spectroscopic analysis in the low-wavelength portion of the spectrum. To facilitate analysis of the UV-region

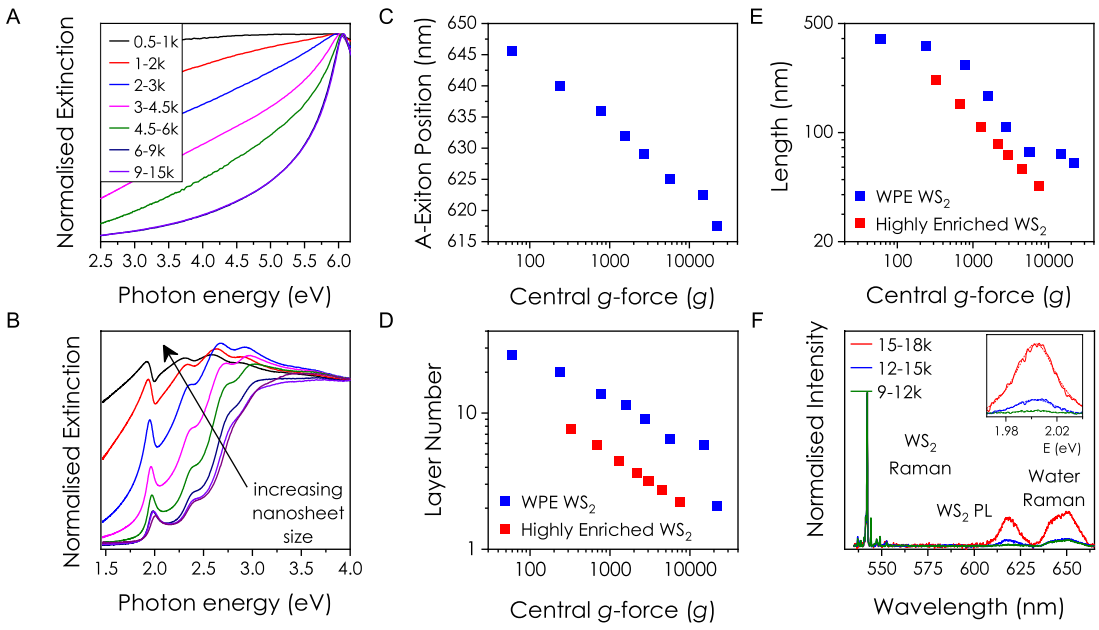

Figure 2. Spectroscopy and size selection. (A) The normalised extinction spectra for whiskey-exfoliated BN nanosheets size-selected at various *g*-forces. (B) The normalised extinction spectra of whiskey-exfoliated WS_2 nanosheets. (C) The shift in A-exciton peak with increasing centrifugation speeds. (D) The layer number as a function of centrifugation speed calculated using the metric from [7]. (E) The length of the WS_2 nanosheets calculated using the A-exciton positions in (C) with the metric from [7]. The 'Highly Enriched WS_2' data in (D) and (E) are also taken from [7]. (F) The Raman spectra for the highest central *g*-force showing PL that scales with centrifugation speed indicating the varying monolayer content.

of the extinction spectra, the BN and WS_2 samples were solvent-exchanged, replacing the whiskey with an aqueous surfactant solution which is transparent to 200 nm. Figure 2(A) shows the extinction spectra of a set of size-selected, whiskey-exfoliated BN samples after transfer into an aqueous surfactant dispersion. All spectra are relatively broad with a long tail extending to low energies and no clear band-edge. This broadening is due to the presence of significant amounts of light scattering contributions to the extinction spectrum (in addition to absorbance) and is typical of wide bandgap nanosheets with dimensions above ~100 nm [30, 31]. It is clear from figure 2(A) that the spectra associated with fractions produced using higher centrifugation speeds display considerably less scattering. As reduced scattering is expected for smaller, thinner nanosheets [30], this data shows that the size-selection procedure is compatible with whiskey-exfoliated samples. We note that the extinction spectrum of the smallest/thinnest fraction reaches half its peak value at 5.5 eV. By comparison with previous data [31], this would imply a nanosheet size and thickness of roughly 400 nm and ten layers, respectively. These values are in the midrange for liquid-exfoliated BN nanosheets but are somewhat larger than the smallest/thinnest BN nanosheets reported in [31].

It is possible to gain more information from optical spectra of the whiskey-exfoliated WS_2 nanosheets. This is because the extinction spectrum is much richer in information, allowing direct extraction of the nanosheet length and thickness [7]. Figure 2(B) shows the normalised extinction spectra for size-selected WS_2 fractions (see Methods and Materials). From this data, it is clear that both spectral shape and A-exciton position change with nanosheet size. Specifically, the shifting A-exciton peak position indicates variations in nanosheet size while the shape changes are associated with size variations due to edge effects [4]. Figure 2(C) shows a consistent blueshift in the peak position of the A-exciton with increasing centrifugation speed, as demonstrated previously for WS_2 in samples exfoliated using water and surfactant [7]. Using a simple metric reported by Backes *et al*, [7] we convert the A-exciton position of the whiskey-exfoliated WS_2 to approximate the nanosheet thickness as shown in figure 2(D) (blue data). We find a significant reduction in nanosheet thickness from ~30 layers at the lowest centrifugation speeds to just a few layers at high speed. Comparing this to previously reported data for WS_2 nanosheets (red data, from [7]) shows whiskey-exfoliation to yield nanosheets which are ~2–3 times thicker than the state-of-the-art surfactant exfoliation methods.

Backes *et al* also reported a metric which allows the nanosheet lateral dimensions to be estimated from the extinction spectra, provided the dimensions of the nanosheets are within certain limits [7]. The lengths calculated are shown in figure 2(E), along with equivalent data also reported by Backes *et al* for surfactant-exfoliated nanosheets. The length of the nanosheets is clearly larger than those exfoliated using an aqueous surfactant solution for a given central *g*-force, again typical of polymer stabilisation [9].

While optical extinction metrics can be used to estimate nanosheet dimensions, they cannot be used to ascertain whether monolayers have definitively been produced. The presence of mono-

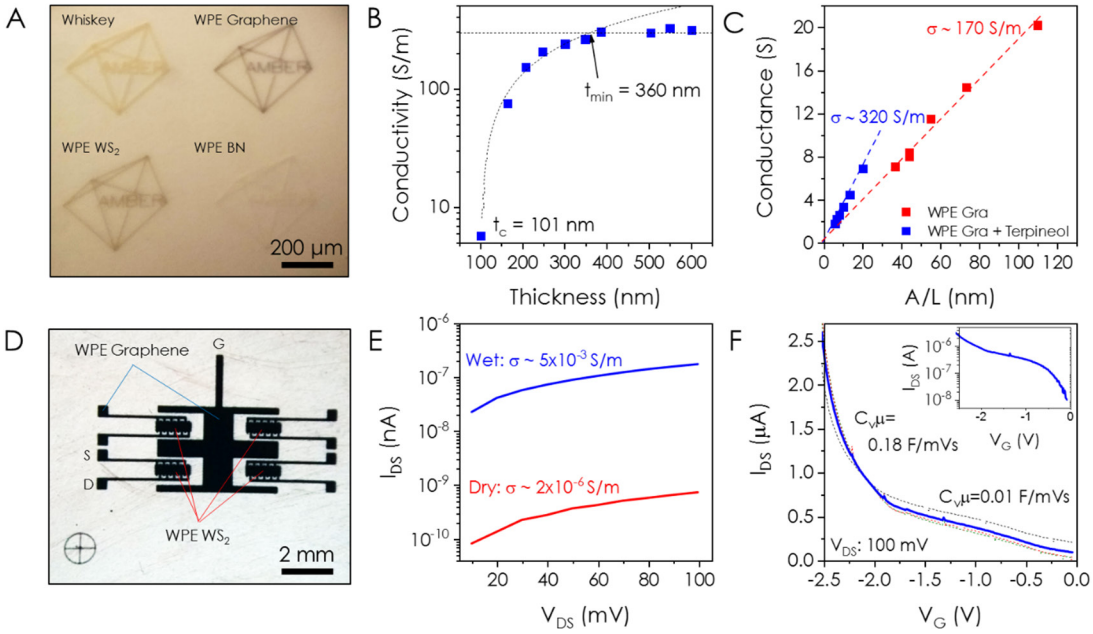

Figure 3. Printed whiskey-exfoliated devices. (A) The AMBER centre logo printed using plain whiskey, WPE graphene, WPE WS_2 and WPE BN. (B) The percolation scaling of WPE graphene (+2.5 vol% terpineol) conductivity with thickness. The fitted parameters give a critical thickness of 101 nm, minimum thickness for bulk behaviour of 360 nm and a percolation exponent of 0.84. (C) The conductance of various printed lengths of WPE graphene and WPE graphene with 2.5 vol% terpineol to extract the conductivity of each ink. (D) An optical micrograph of a side-gated TFT array. The large central gate electrode (G) and the source (S) and drain (D) electrodes are printed using WPE graphene and the channel is printed with WPE WS_2. Each of the four IDEs have a channel length of 70 μm and a width of 7.2 mm. (E) Output curves for the WPE WS_2 channel before (dry) and after (wet) the IL is added. (F) Transfer curve for a WPE WS_2 network gated with EMIm TFSI. The dotted lines represent individual transfer curves and the solid blue line represents the average of four devices. Inset is the same data on a semi-log plot.

layers is typically confirmed via the observation of photoluminescence, typically using a Raman spectrometer where the PL appears at high wavenumbers [7, 9]. Figure 2(H) shows a Raman/PL spectra normalised to the WS_2 2LA(M) mode for 3 of the highest centrifuged samples (i.e. the smallest, thinnest nanosheets). PL peaks consistent with WS_2 are observed at ~620 nm with the Raman signature of water also visible at approximately 650 nm. The PL spectra are also plotted against photon energy in the inset and show narrow symmetric peaks centred around 2.003 eV with FWHM ~43 meV. Such a low value indicates that the monolayers are not heavily doped and largely defect-free [7]. This confirms that good quality nanosheets can be created in complex liquid environments.

Printed transistors composed of networks of WPE graphene and WPE WS_2 nanosheets

To demonstrate the printability of these WPE inks they were directly deposited onto on a paper substrate using an aerosol jet printer (see Methods and Materials). Figure 3(A) shows the AMBER centre logo aerosol jet-printed using neat whiskey and each of the WPE dispersions. We would expect that such networks demonstrate conductive, semiconductive and insulating behaviour for graphene, WS_2 and BN respectively. This would allow WPE-graphene to be used as electrodes in combination with WPE-WS_2 as channel material.

It is necessary to first ensure that printed networks are fully developed and display bulk-like conductivity to confer reproducibility across devices. It is well-known solution-processed nanostructured networks tend to display conductivities which evolve with thickness according to percolation theory before saturating at a bulk-like conductivity above a certain thickness [32]. Figure 3(B) shows a semi-log plot of network conductivity against network thickness where we see a sharp increase in conductivity at the percolation threshold ($t_c \sim 100$ nm) before steadily increasing with thickness, reaching the bulk value of 320 S m^{-1} for thicknesses above 360 nm. The intermediate behaviour is described by percolation theory where conductivity goes with network thickness as $\sigma \propto (t - t_c)^n$ where n is the percolation exponent. Fitting these data gives a t_c of 101 nm and n of 0.84. This data shows that to ensure bulk-like conductivity, WPE-graphene networks must be thicker than 360 nm.

To assess the conductivity (σ) of patterned structures of WPE graphene, lines of thickness, $t = 700$ nm and width, $w = 100$ μm were printed at various lengths, L, and their conductance (G) measured with the expectation that $G = \sigma wt/L$. We note that the wetting characteristics of the inks can be improved by adding viscosity modifiers such as terpineol to the dispersion [1, 33, 34]. Figure 3(B) shows the conductance results of a WPE graphene ink and a WPE graphene ink with 2.5 vol% of terpineol where the presence of the additive confers a factor of two increase in

the conductivity, from 170 to 320 S m^{-1}. This value is only an order of magnitude lower than an inkjet-printed graphene ink with similar nanosheet dimensions [35] which is notable given the organic residues present in the network.

The ability to print nanosheet networks of graphene and WS_2 allows us to fabricate electronic devices solely using nanosheets. Here we fabricate electrolytically gated thin-film transistors both to demonstrate working devices and to assess the electrical characteristics of a WPE semiconducting nanosheet network. The use of an electrolyte, or an ionic liquid (IL), has been demonstrated to be critical for the efficient gating of such networks as electrical double layers form throughout the network under a gate bias [14]. A side-gate array was printed in the design shown in figure 3(D) using WPE graphene with 2.5% terpineol. This design features a large central gate with four interdigitated electrodes (IDEs) nested around it. The IDEs were printed with a channel length of 70 μm and a width of 7.2 mm. An approximately 3 μm thick layer of WPE-WS_2 was then printed across the IDE to form the semiconducting channel. A Raman spectrum of the printed WPE WS_2 is shown in figure S3 where the E_{2g} and A_{1g} modes are clearly visible against the whiskey profile previously shown in figure 1(E). A drop of EMIm TFSI IL was then dropcast onto the array, covering the central area (an optical image is shown in figure S4), to complete the device. Figure 3(E) shows a semi-log plot comparing the conductivity of the WPE WS_2 network before (dry) and after (wet) the IL was placed on the array (linear plots for each are shown in figure S5). Prior to the addition of the IL, the conductivity of the WS_2 network is ~2×10^{-6} S m^{-1}. This value is almost two orders of magnitude lower than similar films of WS_2 (9.4×10^{-5} S m^{-1} [14], 1×10^{-4} S m^{-1} [27]), although it is remarkably comparable to similar films of MoS_2 (5×10^{-6} S m^{-1} [14], 2.5×10^{-6} S m^{-1} [35], 7×10^{-7} S m^{-1} [36]). After the IL is deposited into the network, the conductivity increases by ~3 orders of magnitude, in line with previous reports [14, 27]. This is attributed to residual doping by accumulations of EMIm or TFSI on the basal plane even in the absence of a gate voltage.

The behaviour of the TFTs under a gate bias is shown in figure 3(F). The dotted lines represent individual devices demonstrating the reproducibility across networks, with the solid blue representing their average. We see that the current can be modulated across two orders of magnitude (shown inset, on:off ~340) with a p-type characteristic and two transport regimes. These regimes are fitted using the standard transistor equation for electrolytically gated nanosheet networks

$$I_{DS} = \frac{wt}{L} C_V \mu \left(V_G - V_T\right) V_{DS}$$

where C_V is the volumetric capacitance of the network, μ is the network mobility and the other symbols have their usual meaning. As the measurement of the volumetric capacitance is non-trivial and sensitive to many factors, the product $C_V\mu$ is used as the figure of merit for assessing such electrolytically gated films [14, 37, 38]. The low gate bias regime has a $C_V\mu$ value of ~0.01 F mV^{-1} s^{-1}, with a higher value of ~0.18 F mV^{-1} s^{-1} seen in the higher voltage regime. We attribute the differences in regimes to the hindrance of double layer build up due to the presence of whiskey-originating organic compounds. This results in poor current modulation at low gate voltages until a more complete double layer is formed at higher gate biases. Using the previously reported C_V for WS_2 nanosheets of comparable dimensions (1.2 F cm^{-3}, [14]), we can estimate the mobility of the WPE-WS_2 at 1.5×10^{-3} cm^2 V^{-1} s^{-1}. Although this value is low compared to the state-of-the-art for nanosheet networks, it is still comparable to some pristine organic TFTs [39–41] which speaks to robustness of using nanosheets in thin-film transistors. As the reporting on printed nanosheet-network transistors is still in its infancy, the values reported here should represent a performance floor for future work.

Conclusions

We have demonstrated that nanosheets of layered crystals can be exfoliated and stabilised in Irish whiskey, an ethanol/water mixture infused with esters, aldehydes, fusel alcohols and various kinds of acid. In particular, the mass of nanosheets exfoliated using whiskey is much higher than those exfoliated using an ethanol/water blend. The PL signature of exfoliated WS_2 also demonstrates that monolayers can be produced in a complex liquid environment where the FWHM of the PL peak indicates that the nanosheets are undoped and defect-free. The whiskey dispersions were printed using an aerosol jet printer into electrolytically gated thin-film transistors with on:off ratios of ~340 and $C_V\mu$ of ~0.01 F mV^{-1} s^{-1} for low gate voltages and ~0.18 F mV^{-1} s^{-1} at higher gate biases. The ability to modulate current in a network filled with additives points to the robust nature of the electronic properties of nanosheet networks.

Methods and materials

Materials

The bulk powders were used as-bought; the graphite purchased from Asbury (Grade 3763), the tungsten sulphide from Sigma (CAS: 12138-09-9) and the molybdenum sulphide from Sigma (CAS: 1317-33-5). The whiskey was sponsored by The Teeling Whiskey Co. (Teeling Small Batch, 46% ABV, finished in a rum cask and bottled 12/2017). The NMP (Sigma, CAS:

872-50-4) and ethanol (Trinity College Chemical Stores) used were both HPLC grade.

Exfoliation

The WS_2 and BN were sonicated using a horn-tip probe sonicator (Sonics Vibra-cell VCX-750 ultrasonic processor) with 2.4 g of bulk powder in 80 ml of both whiskey and a 46:54 blend of ethanol and water ($C_i = 30\,g\,l^{-1}$). These were sonicated for 6 h at 60% amplitude and pulsed (6 s on, 2 s off). For the whiskey dispersions, 10 ml of whiskey was added after 3 h to replenish the evaporated solvent. For the ethanol/water dispersion, 10 ml of 46:53 vol:vol ethanol/water was added after 3 h to replenish the evaporated solvent. The graphite was sonicated with 2.4 g of bulk powder in 80 ml of NMP ($C_i = 30\,g\,l^{-1}$) for 6 h at 60% amplitude and with a 6 s on, 2 s off pulse. The resulting dispersions were then subjected to liquid cascade centrifugation.

Size-selection

The graphene was size-selected by centrifuging the exfoliated polydispersion at 2 krpm (425.6 g) for 90 min to sediment out all the large particles and unexfoliated material (72 ml in 3 vials). 15 ml of the supernatant was taken from each vial and then centrifuged at 5 krpm (1702.4 g) for 90 min. The resulting supernatant was fully removed and the sediment was then redispersed in 30 ml of either whiskey or ethanol/water.

The WS_2 and BN polydispersions were subjected to liquid cascade centrifugation with sequentially increasing centrifugation speeds following previous reporting [7]. Briefly, an initial centrifugation of 0.5 krpm (26.6 g) for 90 min was performed to remove the unexfoliated material. This supernatant was then centrifuged at 1 krpm (106.4 g) for 90 min after which the sediment was collected (sample '0.5–1 k') with the supernatant then subjected to another centrifugation at 2 krpm (425.6 g) for 90 min. This sediment was collected (sample '1–2 k') with the supernatant again subjected to centrifugation at 3 krpm (957.6 g) for 90 min. This procedure of collecting sediment and centrifuging the supernatant at higher rpm was repeated for 4.5 krpm (2156.6 g), 6 krpm (3830.4 g), 9 krpm (7889.4 g), 12 krpm (14 025 g) and 15 krpm (21 915 g). The redispersion of sediment is especially advantageous as this allows dispersions to be created at arbitrary concentrations meaning the lower mass samples (>6 krpm) can be concentrated for microscopic and spectroscopic analysis. The samples used for printing were those trapped between 1 and 2 krpm as these provided a relatively large quantity of material. The data presented in figure 2 uses the central rpm/g-force of an average of two consecutive centrifugation steps. For example, the sediment collected from the 1 krpm centrifugation had a central rpm of 0.75 krpm (59.8 g).

All samples were centrifuged in a Hettich Mikro 220R, using 28 ml vials with the fixed-angle rotor 1016 for *g*-forces up to 3830.3 g, and using 1.5 ml vials with the fixed-angle rotor 1195-A for *g*-forces greater than 3830.3 g.

Concentration measurements

The data in figure 1(D) was created following the exfoliation procedures above (*N.B.* the graphite was exfoliated in NMP and transferred to whiskey or ethanol/water whereas the WS_2 and BN were exfoliated directly in either whiskey or ethanol/water). In each case, 72 ml of the post-sonication polydispersion was size-selected between 1 and 2 krpm (106.4 g and 425.6 g) in three 28 ml vials and the sediment was redispersed in either 30 ml of whiskey or 30 ml of ethanol/water (10 ml per vial). The vials were then bath-sonicated for 30 min to redisperse the material. The concentration of each sample was measured by filtration through an alumina membrane (Whatman Anodisc 47 mm, pore size = 20 nm) and weighing. The concentrations were measured 1 h after bath sonication.

Optical characterisation

The sedimentation profiles in figure 1(D) were taken with a homemade apparatus using an array of synchronized pulsed lasers and photodiodes. The transmission of laser pulses ($\lambda = 650$ nm, duration = 10 ms) through the centre of a quartz cuvette was monitored for 168 h.

Optical extinction was measured on a Varian Cary 500 in quartz cuvettes in 1 nm increments. The plethora of organic compounds present in whiskey means there is strong absorption for wavelengths <310 nm (See figure S2). To obtain the full extinction spectra in figures 2(B) and (D), the whiskey-exfoliated WS_2 and BN nanosheets were centrifuged at high speed (18 krpm, 31 557.6 g) for 90 min and the sediment was redispersed in an aqueous surfactant solution (sodium cholate, $2\,g\,l^{-1}$) for analysis.

Raman and photoluminescence spectroscopy was performed on the liquid dispersions using a Horiba Jobin Yvon LabRAM HR800 with 532 nm excitation laser in air under ambient conditions. The Raman/PL emission was collected by 100× objective lens (N.A. = 0.8) and dispersed by $600\,g\,mm^{-1}$ at 25% of the laser power (~5 mW). The measurements were performed following the procedure outlined previously [9]. From [9]: A drop (~40 μl) was placed on a glass slide and the drop edge was optically focused using a 10× objective. The focus for the measurement with the 100× objective was readjusted in such a way that the laser was focused slightly above the drop. Focusing inside the drop leads to inner filter and reabsorption effects and causes the WS_2 PL to be asymmetric. It was noted that measurements taken close to the drop edge were more reliable than in the centre of the drop because the focus remained constant throughout the measurement due to the lower curvature of the drop and hence negligible changes in the focus by evaporation of water. An average of ~5 measurements

was displayed. To follow the drying of a drop, 10% of the laser power was used to avoid sample heating in the dried state. The laser was switched off after a measurement was acquired and the focus was readjusted prior to each measurement.

TEM characterisation

Bright field transmission electron microscopy imaging was performed using a JEOL 2100, operated at 200 kV. Holey carbon grids (400 mesh) were purchased from Agar Scientific and prepared by diluting dispersion to a low concentration and drop casting onto a grid placed on a filter membrane to wick away excess solvent.

Aerosol jet printing

The aerosol jet printer is an Optomec AJP 300. A 150 μm nozzle was used for printing with sheath and carrier flow rates set to 40 $\pm$ 3 and 25 $\pm$ 3 sccm, respectively. The temperature of the chiller used to cool the ink was set to 20 C and the platen was set to 60 C. The WS_2 and BN dispersions selected for use an ink were those size-selected between 1 and 2 krpm. 2 ml of each ink was used at a time with the atomiser current set to ~0.5 A. All printing was performed at platen speeds of 1 mm s^{-1}. The samples were then dried in a vacuum oven overnight at 80 C to remove any trapped solvent. The TFT arrays were printed onto an alumina-coated PET substrate (Mitsubishi Paper Mills, NB-TP-3GU100 A4). Prior to use, the substrate was rinsed in DI water and cleaned in an IPA in a sonic bath for 10 min and blown dry with N_2. The patterns in figure 3(A) were printed on PEL P60 paper available from Printed Electronics. The sample thickness was measured using contact profilometry.

Electrical characterisation

1-Ethyl-3-methylimidazolium bis(trifluoromethylsulfonyl)imide [Sigma Aldrich] was dried in a vacuum oven for 24 h at a temperature of 70 °C. The electrical measurements were performed using a Keithley 2612A under high vacuum in a Janis probe station. This is to prevent water uptake in the IL which would reduce the electrochemical window. To remove any water which may have been absorbed while placing the device into the chamber, the device was heated to 70 °C for 12 h at 10^{-4} mbar.

Acknowledgments

We wish to thank the Teeling Whiskey Company for supplying solvents. This work was primarily funded through the ERC Advanced Grant FUTUREPRINT. We also acknowledge support from the European Union Seventh Framework Program under grant agreements 604391 and 785219 Graphene Flagship and the Science Foundation Ireland (SFI) funded centre AMBER (SFI/12/RC/2278). The devices were manufactured using facilities in the Additive Research Laboratory at the AMBER centre, CRANN Institute, Trinity College Dublin, Ireland. The AR-Lab is an SFI supported research centre.

ORCID iDs

Adam G Kelly https://orcid.org/0000-0002-6070-7070
Victor Vega-Mayoral https://orcid.org/0000-0001-8626-0775
Jonathan N Coleman https://orcid.org/0000-0001-9659-9721

References

[1] Bonaccorso F, Bartolotta A, Coleman J N and Backes C 2016 2D-crystal-based functional inks *Adv. Mater.* **28** 6136–66
[2] Coleman J N *et al* 2011 Two-dimensional nanosheets produced by liquid exfoliation of layered materials *Science* **331** 568–71
[3] Hernandez Y *et al* 2008 High-yield production of graphene by liquid-phase exfoliation of graphite *Nat. Nanotechnol.* **3** 563–8
[4] Backes C *et al* 2014 Edge and confinement effects allow *in situ* measurement of size and thickness of liquid-exfoliated nanosheets *Nat. Commun.* **5** 4576
[5] Hu G *et al* 2017 Black phosphorus ink formulation for inkjet printing of optoelectronics and photonics *Nat. Commun.* **8** 278
[6] Harvey A *et al* 2017 Exploring the versatility of liquid phase exfoliation: producing 2D nanosheets from talcum powder, cat litter and beach sand *2D Mater.* **4** 025054
[7] Backes C *et al* 2016 Production of highly monolayer enriched dispersions of liquid-exfoliated nanosheets by liquid cascade centrifugation *ACS Nano* **10** 1589–601
[8] Lotya M *et al* 2006 Liquid phase production of graphene by exfoliation of graphite in surfactant/water solutions *J. Am. Chem. Soc.* **131** 3611–20
[9] Vega-Mayoral V *et al* 2016 Photoluminescence from liquid-exfoliated WS_2 monomers in poly(vinyl alcohol) polymer composites *Adv. Funct. Mater.* **26** 1028–39
[10] Yu X, Prévot M S and Sivula K 2014 Multiflake thin film electronic devices of solution processed 2D MoS_2 enabled by sonopolymer assisted exfoliation and surface modification *Chem. Mater.* **26** 5892–9
[11] Li J *et al* 2013 Efficient inkjet printing of graphene *Adv. Mater.* **25** 3985–92
[12] McManus D *et al* 2017 Water-based and biocompatible 2D crystal inks for all-inkjet-printed heterostructures *Nat. Nanotechnol.* **12** 343–50
[13] Withers F *et al* 2014 Heterostructures produced from nanosheet-based inks *Nano Lett.* **14** 3987–92
[14] Kelly A G *et al* 2017 All-printed thin-film transistors from networks of liquid-exfoliated nanosheets *Science* **356** 69–72
[15] Carey T *et al* 2017 Fully inkjet-printed two-dimensional material field-effect heterojunctions for wearable and textile electronics *Nat. Commun.* **8** 1202
[16] Hughes J M, Aherne D and Coleman J N 2013 Generalizing solubility parameter theory to apply to one- and two-dimensional solutes and to incorporate dipolar interactions *J. Appl. Polym. Sci.* **127** 4483–91
[17] Wang H *et al* 2012 Integrated circuits based on bilayer MoS_2 transistors *Nano Lett.* **12** 4674–80
[18] Zhou K-G, Mao N-N, Wang H-X, Peng Y and Zhang H-L 2011 A mixed-solvent strategy for efficient exfoliation of inorganic graphene analogues *Angew. Chem., Int. Ed. Engl.* **50** 10839–42
[19] Conner J M, Paterson A, Birkmyre L and Piggott J R 1999 Role of organic acids in maturation of distilled spirits in oak casks *J. Inst. Brew.* **105** 287–91
[20] Reazin G H 1981 Chemical mechanisms of whiskey maturation *Am. J. Enol. Viticult.* **32** 283–9

[21] MacNamara K, van Wyk C J, Augustyn O P H and Rapp A 2017 Flavour components of whiskey. II ageing changes in the high-volatility fraction *South Afr. J. Enol. Viticul.* **22** 75–81
[22] Piggott J R, Conner J M and Paterson A 1995 Flavour development in whisky maturation **37** 1731–51
[23] May P, Khan U, Hughes J M and Coleman J N 2012 Role of solubility parameters in understanding the steric stabilization of exfoliated two-dimensional nanosheets by adsorbed polymers *J. Phys. Chem.* C **116** 11393–400
[24] Abdullah A H, Ismail Z, Zainal Abidin A S and Yusoh K 2019 Green sonochemical synthesis of few-layer graphene in instant coffee *Mater. Chem. Phys.* **222** 11–9
[25] Ismail Z *et al* 2017 Black tea assisted exfoliation using a kitchen mixer allowing one-step production of graphene *Mater. Res. Express* **4** 075607
[26] Perumal S, Park K T, Lee H M and Cheong I W 2016 PVP-b-PEO block copolymers for stable aqueous and ethanolic graphene dispersions *J. Colloid Interface Sci.* **464** 25–35
[27] O'Suilleabhain D, Vega-Mayoral V, Kelly A G, Harvey A and Coleman J N 2019 Percolation effects in electrolytically gated WS_2/graphene nano:nano composites *ACS Appl. Mater. Interfaces* **11** 8545–55
[28] Ogilvie S P *et al* 2017 Considerations for spectroscopy of liquid-exfoliated 2D materials: emerging photoluminescence of N-methyl-2-pyrrolidone *Sci. Rep.* **7** 16706
[29] Nguyen E P *et al* 2014 Investigation of two-solvent grinding-assisted liquid phase exfoliation of layered MoS_2 *Chem. Mater.* **27** 53–9
[30] Harvey A *et al* 2018 Non-resonant light scattering in dispersions of 2D nanosheets *Nat. Commun.* **9** 4553
[31] Griffin A *et al* 2018 Spectroscopic size and thickness metrics for liquid-exfoliated h-BN *Chem. Mater.* **30** 1998–2005
[32] De S, King P J, Lyons P E, Khan U and Coleman J N 2010 Size effects and the problem with percolation in nanostructured transparent conductors *Acs Nano* **4** 7064–72
[33] Mahajan A, Frisbie C D and Francis L F 2013 Optimization of aerosol jet printing for high-resolution, high-aspect ratio silver lines *ACS Appl. Mater. Interfaces* **5** 4856–64
[34] Rother M *et al* 2017 Aerosol-jet printing of polymer-sorted (6,5) carbon nanotubes for field-effect transistors with high reproducibility *Adv. Electron. Mater.* **3** 1700080
[35] Finn D J *et al* 2014 Inkjet deposition of liquid-exfoliated graphene and MoS_2 nanosheets for printed device applications *J. Mater. Chem.* C **2** 925–32
[36] Cunningham G *et al* 2012 Percolation scaling in composites of exfoliated MoS_2 filled with nanotubes and graphene *Nanoscale* **4** 6260
[37] Higgins T M *et al* 2018 Electrolyte-gated n-type transistors produced from aqueous inks of WS_2 nanosheets *Adv. Funct. Mater.* **29** 1804387
[38] Rivnay J *et al* 2015 High-performance transistors for bioelectronics through tuning of channel thickness *Sci. Adv.* **1** e1400251
[39] Diallo A K *et al* 2011 Top gate copper phthalocyanine thin film transistors with laser-printed dielectric *Synth. Met.* **161** 888–93
[40] Al-Hashimi M *et al* 2011 Synthesis, characterization, and field effect transistor properties of regioregular poly(3-alkyl-2,5-selenylenevinylene) *Macromolecules* **44** 5194–9
[41] Zielke D *et al* 2005 Polymer-based organic field-effect transistor using offset printed source/drain structures *Appl. Phys. Lett.* **87** 123508